THE ASTROPHYSICAL JOURNAL, 522:524–539, 1999 September 1

SPECTRAL LINES FOR POLARIZATION MEASUREMENTS OF THE CORONAL MAGNETIC FIELD. II. CONSISTENT TREATMENT OF THE STOKES VECTOR FOR MAGNETIC-DIPOLE TRANSITIONS

R. CASINI AND P. G. JUDGE
High Altitude Observatory, National Center for Atmospheric Research,[1] P.O. Box 3000, Boulder, CO 80307-3000
Received 1998 November 20; accepted 1999 April 2

ABSTRACT

We present a compact, self-consistent formulation for the description of polarized radiation from magnetic-dipole transitions occurring in the magnetized solar corona. This work differs from earlier treatments by Sahal-Bréchot and House in the 1970s, in that the radiative emission coefficients for the four Stokes parameters, I, Q, U, and V, are treated to first order in a Taylor expansion of the line profile in terms of the Larmor frequency of the coronal magnetic field. In so doing, the influence on the scattered radiation of both atomic polarization, induced through anisotropic irradiation, and the Zeeman effect is accounted for in a consistent way. It is found that the well-known magnetograph formula, relating the V profile to the frequency derivative of the I profile, must be corrected in the presence of atomic alignment produced by anisotropic irradiation. This correction is smallest for lines where collisions and cascades dominate over excitation by anisotropic radiation, but it systematically increases with height above the solar limb (up to a theoretical maximum of 100%, in the collisionless regime and in the limit of vanishing longitudinal magnetic field). Although the correction to the magnetograph formula must be calculated separately for each line as a function of heliocentric distance, it is likely to be small for some lines of practical interest, along lines of sight close to the solar limb.

Subject headings: line: formation — Sun: atmosphere — Sun: corona — Sun: magnetic field

1. INTRODUCTION

Over a century ago, eclipse data showed the presence in the solar corona of looplike structures reminiscent of magnetic-field patterns seen in the laboratory. Now we know that magnetic fields emerging from solar subphotospheric layers, buffeted by photospheric convective motions, control the dynamics and heating of the corona. However, in spite of enormous strides in our ability to determine vector magnetic fields in the photosphere and properties of the plasma in the corona, our ability to determine properties of the coronal magnetic fields remains severely limited. Away from strong fields associated with active regions, few useful measurements of coronal fields exist because they are extremely difficult to make. This is simply because the fields in the quiet-Sun corona are intrinsically weak (~ 10 G) and their influence on the electromagnetic radiation emitted by the coronal plasma is correspondingly weak.

It is important to try to determine coronal magnetic fields observationally for some fundamental reasons. First, the basic physical conditions change enormously from the photosphere to corona. In the photosphere, where almost all magnetic-field measurements are made, the plasma is in a forced, high-β state in which magnetic fields are confined by convective motions to small tubelike structures filling only a small fraction of the available volume. In the corona, momentum balance ensures that the field must be almost in a force-free, low-β state, filling all of the available volume. Second, there is still debate concerning the basic MHD of the coronal plasma in response to the "driving motions" at the photospheric level. Does the corona evolve such that current sheets form naturally and abundantly, as suggested by Parker's fundamental theorem of magnetostatics (Parker 1994), or do processes occur to avoid such configurations (Van Ballegooijen 1985)? Both of these points indicate that magnetic-field extrapolation from photospheric measurements cannot presently be trusted, without even acknowledging the fact that the extrapolation problem is very poorly posed (e.g., Low & Lou 1990). Thus, it is important to obtain more direct measurements of properties of the coronal magnetic field.

At present, observations of two kinds offer the best opportunities to determine properties of the coronal magnetic field, radio observations and observations of the well-known coronal forbidden emission lines (see, e.g., the introduction of Judge 1998). The purpose of the present paper is to provide a consistent theoretical treatment of the latter, containing the essential physics of the formation of the polarized emission lines under the influence of both anisotropic radiation and the Zeeman effect. This paper focuses on the radiative contribution to the statistical equilibrium of the radiating atom. Collision analysis for specific lines of interest will be deferred to future papers.

1.1. *Historical Overview and Statement of the Problem*

The 1960s marked a starting point for the spectroscopic diagnosis of coronal magnetic fields using magnetic dipole (M1) coronal emission lines in two distinct ways. First, Charvin (1965; see also Hyder 1965; Perche 1965a, 1965b) showed how measurements of the linear polarization of these lines can be related to the direction of the magnetic field projected onto the plane of the sky (POS). This effect arises because the corona is irradiated anisotropically by the photosphere, so that atomic polarization is induced in the radiating atom (see § 3.2). Second, Harvey (1969) attempted to use circular-polarization measurements of the coronal green line (Fe XIV λ5304) to determine the strength of the line-of-sight (LOS) component of the

[1] The National Center for Atmospheric Research is sponsored by the National Science Foundation

magnetic field, through the Zeeman effect. However, the technical difficulties encountered by Harvey (1969) were of a magnitude that this longitudinal Zeeman effect has even now yet to be detected convincingly in M1 coronal emission lines, although a mildly interesting upper limit of 40 G was obtained under nonoptimal conditions by Kuhn (1995). This indicates that measurements will yield detections of the longitudinal Zeeman effect in the near future.

The work of Charvin (1965) helped to inspire two groups to develop coronal polarimetry, both observationally and theoretically, over the following two decades. A coronal emission-line polarimeter, designed to observe linear polarization in the M1 emission lines of Fe XIII at 10747 and 10798 Å, was built and operated by a joint High Altitude Observatory/National Solar Observatory (HAO/NSO) team. Successful results for the orientation of the magnetic field in the POS and comparisons between computed and measured degrees of polarization are discussed by Querfeld & Smartt (1984) and Arnaud & Newkirk (1987). Similar results for an instrument observing the coronal green line, operated at Pic-du-Midi Observatory, are described by Arnaud (1982).

Theoretical work developed along with observational work. Two important steps were taken in the 1970s. First, Sahal-Bréchot (1974, 1977) and House (1977) included collisional terms in the description of the statistical equilibrium of the radiating atom. Second, in Sahal-Bréchot (1977), use was made of the powerful formalism based on the multipolar expansion of the density matrix of the radiating atom over the basis of the irreducible spherical tensor operators (e.g., Brink & Satchler 1968; Blum 1981). In fact, this choice of basis, rather than the standard basis built from the atomic-Hamiltonian eigenstates, is the most appropriate for the description of atomic polarization, because of the direct physical meaning that can be attributed to the various multipole orders of the irreducible spherical tensors, which will be illustrated by the symmetry and invariance properties of multipoles to be discussed in this paper (see §§ 2.1, 2.4, 3.1, and 3.3). In addition, the polarization properties of the emitted radiation are expressed in their simplest form in that basis.

A limit in previous theoretical treatments of the formation of M1 coronal lines in the presence of magnetic fields is that the circular polarization (V profile) was explicitly assumed to be zero. This is consistent to zeroth order in a Taylor expansion of the line profile in terms of the Larmor frequency of the coronal magnetic field, assuming that first-order effects (i.e., the longitudinal Zeeman effect) be completely negligible (see § 2.3). For this reason, and also because of the technical difficulties in measuring the Stokes profiles as functions of frequency, all previous theoretical work on the problem of M1 coronal emission lines focused only upon linear polarization and frequency-integrated line profiles. On the other hand, the few observational attempts to detect the longitudinal Zeeman effect in those lines (Harvey 1969; Kuhn 1995) aimed at an interpretation based on the well-known "magnetograph formula" (see § 4, eq. [40]), relating the V profile to the frequency derivative of the I profile, without addressing the physics of resonance scattering. These two approaches have historically been used independently of one another. In reality, they should be treated together, as both resonance-scattering linear polarization and Zeeman-effect circular polarization can be affected by atomic polarization. The purpose of the present paper is to provide a consistent treatment of both linear and circular polarizations of M1 coronal lines by extending previous theoretical treatments with the inclusion of first-order magnetic effects on the line profile.

We adopt the nonrelativistic quantum theory of line formation under the hypothesis of complete redistribution of frequency, put forward in the 1980s by Landi Degl'Innocenti in a series of papers (Landi Degl'Innocenti 1983, 1984, 1985, hereafter LA83, LA84, and LA85, respectively). The formalism of the irreducible spherical tensors is easily implemented in the theory, so both the former and the new results on the polarization properties of M1 coronal lines can be derived in a straightforward way.

The hypothesis of complete redistribution is equivalent to assuming that the incident radiation has no spectral structure across the spectral range of a radiative transition in the atom (flat-spectrum approximation). This condition is normally satisfied in the frame of reference of the atom, at least for transitions in the IR and in the visible. When the thermal motion of the atoms in the hot corona is taken into account, instead, Doppler redistribution can be an issue. Even in that case, for the highly ionized atomic species of interest, IR and visible transitions generally do not match significant spectral features of the photospheric spectrum. As a notable exception, among the lines predicted to be strong enough for one even to attempt to measure the longitudinal Zeeman effect (see Judge 1998, Table 4), we can cite Fe XIV λ5304. Because of the elevated line density in the UV, partial redistribution could in principle be an issue at shorter wavelengths. However, UV transitions in the corona are largely dominated by collisional excitation and by collisional and/or radiative spontaneous deexcitation, so the UV spectrum from the underlying solar atmosphere does not play an essential role in the statistical equilibrium of the atom.

Before proceeding, we wish to remind readers unfamiliar with the density matrix formalism of two basic facts. First, the density matrix extends the description of an atomic system beyond the simple concept of "populations of the atomic states" (described by the diagonal elements of the density matrix in the standard representation) by introducing the concept of "quantum coherences" between different atomic states (described by the off-diagonal elements of the density matrix in the standard representation). Second, the physics of line formation must be independent of the particular representation adopted for the density matrix, so an entirely equivalent calculation to the one presented here could be done in the standard representation based on the atomic-Hamiltonian eigenstates (see Sahal-Bréchot 1974; House 1977, for the restricted problem of the linear polarization of M1 coronal lines), rather than on the irreducible spherical tensors. However, as already mentioned, the formalism of the irreducible spherical tensors allows us to develop a more compact formulation of the mathematical problem, and a deeper understanding of the physical problem is gained, as the various symmetry and invariance properties of the system stand out clearly.

2. STOKES VECTOR OF THE SCATTERED RADIATION

Most commonly, the forbidden lines that are observed in the solar corona (e.g., the green line of Fe XIV at 5304 Å, the red line of Fe X at 6374 Å, and the infrared lines of Fe XIII at 10747 and 10798 Å) are optically thin emission lines that originate in the M1 transitions $|\Delta J| = 1$ within the ground term, i.e., transitions of the form $(\alpha_0 J) \rightarrow (\alpha_0 J_0)$, where α_0 specifies the atomic

configuration of the ground term (the particular kind of coupling is not of concern here). These lines are excited in the corona both by isotropic collisions with charged particles (through both direct excitation and cascade processes) and by anisotropic radiation from the underlying photosphere, which is reemitted in all directions in the process known as "resonance scattering." The observed lines then carry a polarization signature that is typical of this scattering process. If a magnetic field is present, each level J is split into a series of $2J + 1$ Zeeman substates, distinguished by the magnetic quantum number, M. In that case, the polarization signature is modified with respect to the field-free case, and in principle it carries a complete information on the local vector magnetic field (apart from the well-known 180° ambiguity in the determination of the magnetic-field orientation on the POS; see eqs. [39b] and [39c]).

In general, the transport of polarized radiation is governed by a vector radiative transfer equation of the form (see, e.g., LA83)

$$\frac{d}{ds}\boldsymbol{S} = -\mathbf{M}\boldsymbol{S} + \boldsymbol{E}\,,$$

where $\boldsymbol{S} \equiv (I, Q, U, V)$ is the Stokes vector of the radiation field, $\mathbf{M}$ is the 4×4 absorption matrix, $\boldsymbol{E}$ is the emission vector, and s is the linear coordinate along the LOS. In our case, all lines of interest are optically thin along all LOSs through the corona because of the small oscillator strengths and low column densities of the coronal plasma (both of which contribute to the optical depth, and hence to the norm of the absorption matrix $\mathbf{M}$), so the solution of the radiative transfer equation is simply determined by integrating the emission vector along the LOS. We then need to consider only the emission coefficients $\varepsilon_i(\omega, \hat{\boldsymbol{k}})$ ($i = 0$, 1, 2, and 3, indicating the four Stokes parameters I, Q, U, and V, respectively) at the observed frequency, ω, and for a propagation direction of the scattered radiation, $\hat{\boldsymbol{k}}$, coincident with the LOS.

2.1. *Irreducible Representation of the Emission Coefficients*

Because only the transition $(\alpha_0 J) \rightarrow (\alpha_0 J_0)$ contributes significantly to the scattered radiation from the atom within the line's spectral range, we can safely adopt the expression for the emission coefficients valid in the approximation of the two-level atom. In the frame of reference of the magnetic field (the "B frame"), such that the local vector magnetic field is aligned with the quantization axis (x_3-axis), that expression is given by[2] (cf. Landi Degl'Innocenti, Bommier, & Sahal-Bréchot 1991, eqs. [41] and [36])

$$\begin{aligned}\varepsilon_i(\omega, \hat{\boldsymbol{k}}) = \frac{\hbar\omega}{4\pi}\,\mathcal{N}(2J+1)A(\alpha_0 J \rightarrow \alpha_0 J_0)_{\mathrm{M1}} \sum_{KK',Q} \sqrt{3(2K+1)(2K'+1)}\,\rho^K_Q(\alpha_0 J)\mathcal{T}^{K'}_Q(i, \hat{\boldsymbol{k}})_{\mathrm{M1}} \\ \times \sum_{MM',M_0} \sum_{qq'} (-1)^{J-M_0+Q-1}\,\frac{1}{2}\,[\Phi(\omega_{\alpha_0 JM,\alpha_0 J_0 M_0} - \omega) + \Phi^*(\omega_{\alpha_0 JM',\alpha_0 J_0 M_0} - \omega)] \\ \times \begin{pmatrix} J & J & K \\ M' & -M & -Q \end{pmatrix} \begin{pmatrix} J & J_0 & 1 \\ -M & M_0 & q \end{pmatrix} \begin{pmatrix} J & J_0 & 1 \\ -M' & M_0 & q' \end{pmatrix} \begin{pmatrix} 1 & 1 & K' \\ -q & q' & -Q \end{pmatrix}. \end{aligned} \tag{1}$$

In the above equation, $\mathcal{N}$ is the number density of the radiating ion; $A(\alpha_0 J \rightarrow \alpha_0 J_0)_{\mathrm{M1}}$ is the Einstein coefficient for the spontaneous M1 transition $(\alpha_0 J) \rightarrow (\alpha_0 J_0)$; $\rho^K_Q(\alpha_0 J)$ are the irreducible spherical components of the density matrix (or statistical tensor) of the excited level $(\alpha_0 J)$; $\mathcal{T}^K_Q(i, \hat{\boldsymbol{k}})_{\mathrm{M1}}$ are the irreducible spherical components of suitable geometric tensors, specifying the geometry of the observer (i.e., the LOS, $\hat{\boldsymbol{k}}$, and the orientation of the reference direction for linear-polarization measurement; see Fig. 1) with respect to the frame of reference adopted; and $\Phi(\omega_0 - \omega) = \phi(\omega_0 - \omega) + i\psi(\omega_0 - \omega)$ is the complex line profile centered on ω_0 (in general, ϕ is the Voigt profile and ψ is the associated Faraday-Voigt dispersion function). The last row of equation (1) is a product of four 3-j symbols (see, e.g., Brink & Satchler 1968), which describes the coupling of the multipole orders K and K' with the angular-momentum states J and J_0 of the atom in the upper and lower levels, respectively.

The components of the statistical tensor for a level (αJ), $\rho^K_Q(\alpha J)$ are related to the elements of the density matrix in standard representation, $\rho_{\alpha J}(M, M')$, through the formula (e.g., LA84, eq. [28])

$$\rho^K_Q(\alpha J) = \sum_{MM'} (-1)^{J-M}\sqrt{2K+1} \begin{pmatrix} J & J & K \\ M' & -M & Q \end{pmatrix} \rho_{\alpha J}(M, M')\,. \tag{2}$$

The multipole order of the statistical tensor $\rho^K_Q(\alpha J)$ is therefore restricted to the values $K = 0, \ldots, 2J$, because of the 3-j symbol in equation (2). In particular we note that

$$\rho^0_0(\alpha J) = \frac{1}{\sqrt{2J+1}} \sum_M \rho_{\alpha J}(M, M)\,. \tag{3}$$

Therefore, if the normalization of the density matrix in standard representation is chosen so that $\rho_{\alpha J}(M, M)$ represents the probability of finding the atomic system in the sublevel (αJM), then $(2J + 1)^{1/2}\rho^0_0(\alpha J)$ gives the total probability of occupancy (i.e., the population) of the level (αJ). Because of the condition $M' - M + Q = 0$, implied by the 3-j symbol in equation (2), we also see that for a completely diagonal density matrix (in standard representation) the only nonvanishing components of the

[2] Please note that in the following equation Q indicates the components of the irreducible spherical tensors of order K and K', not the Stokes Q parameter. Throughout this paper, the context should always be clear enough to understand the current use of the symbol Q.

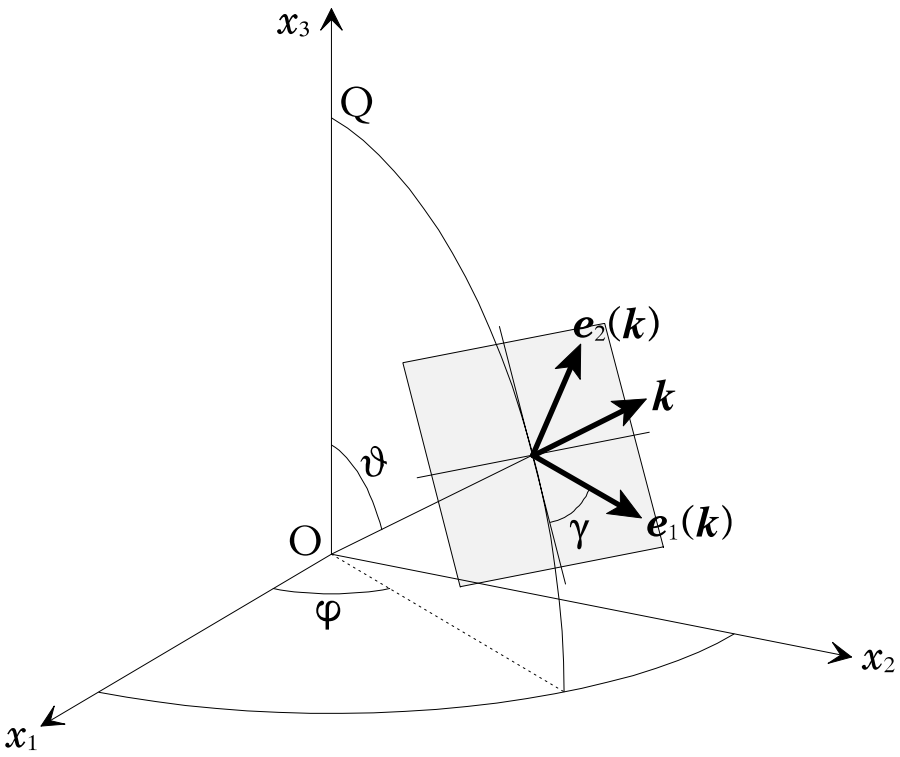

FIG. 1.—Geometry of the observer in the frame of reference adopted. The plane of polarization, generated by the basis vectors for linear polarization, $\boldsymbol{e}_1(\boldsymbol{k})$ and $\boldsymbol{e}_2(\boldsymbol{k})$, is normal to the propagation vector, $\boldsymbol{k}$ (unit vector $\hat{\boldsymbol{k}}$). The position angle γ fixes the reference direction for linear-polarization measurements, $\boldsymbol{e}_1(\boldsymbol{k})$, along which $\frac{1}{2}(I + Q)$ is measured.

statistical tensor are those with $Q = 0$. In this particular case, a direct evaluation of the 3-j symbol involved in equation (2) shows that the orientation and alignment of the level (αJ) are respectively described by the multipole orders (cf. Sahal-Bréchot 1977, eqs. [11] and [12])

$$\rho^1_0(\alpha J) = \frac{\sqrt{3}}{\sqrt{J(J+1)(2J+1)}} \sum_M M \rho_{\alpha J}(M, M) \tag{4}$$

and

$$\rho^2_0(\alpha J) = \frac{\sqrt{5}}{\sqrt{J(J+1)(2J+1)(2J-1)(2J+3)}} \sum_M [3M^2 - J(J+1)] \rho_{\alpha J}(M, M) \, . \tag{5}$$

The geometric tensors, $\mathcal{T}^K_Q(i, \hat{\boldsymbol{k}})_{\mathrm{M1}}$, are given in Table 1. They are related to the analogous tensors $\mathcal{T}^K_Q(i, \hat{\boldsymbol{k}})_{\mathrm{E1}}$ (originally introduced in LA83; see Appendix I in that paper), entering the expression of the emission coefficients for electric-dipole (E1) transitions, through the equations

$$\mathcal{T}^K_Q(i, \hat{\boldsymbol{k}})_{\mathrm{M1}} = \begin{cases} \mathcal{T}^K_Q(i, \hat{\boldsymbol{k}})_{\mathrm{E1}} & \text{for } i = 0, 3 \, , \\ -\mathcal{T}^K_Q(i, \hat{\boldsymbol{k}})_{\mathrm{E1}} & \text{for } i = 1, 2 \, . \end{cases} \tag{6}$$

(This relation is ultimately determined to the pseudovector character of the radiation magnetic field entering the interaction Hamiltonian.) The multipole order of the geometric tensors $\mathcal{T}^K_Q(i, \hat{\boldsymbol{k}})_{\mathrm{M1}}$ is restricted to the values $K = 0,1,2$ only, because of the dipole character of the transitions considered (see last 3-j symbol of eq. [1]).

The most relevant property of the irreducible representations of the statistical and geometric tensors is the physical invariance of their multipole orders under transformation of the coordinate system. In fact, if S and S' are two different frames of reference connected by the Eulerian rotation $R_{SS'}$, the irreducible spherical components of the statistical and geometric tensors in S and S' are related by (e.g., LA84, eqs. [31] and [A18])

$$(\rho^K_Q)_{S'} = \sum_{Q'} [\mathcal{D}^K_{Q'Q}(R_{SS'})]^* (\rho^K_{Q'})_S \, , \tag{7a}$$

$$(\mathcal{T}^K_Q)_{S'} = \sum_{Q'} \mathcal{D}^K_{Q'Q}(R_{SS'}) (\mathcal{T}^K_{Q'})_S \, , \tag{7b}$$

where $\mathcal{D}^K_{Q'Q}(R_{SS'})$, $K = 0,1,2$, are the rotation matrices associated with the transformation $R_{SS'}$ (e.g., Brink & Satchler 1968). In particular, if a given multipole K vanishes identically (i.e., all associated Q components are vanishing) in a particular frame of reference, then it identically vanishes in any frame of reference.

TABLE 1

EXPRESSIONS OF THE GEOMETRIC TENSORS $\mathcal{T}^K_Q(i, \hat{\boldsymbol{k}})_{\mathrm{M1}}$

$\mathcal{T}^K_Q(i, \hat{\boldsymbol{k}})_{\mathrm{M1}}$	Expression
	$\mathcal{T}^K_Q(0, \hat{\boldsymbol{k}})_{\mathrm{M1}}$
$\mathcal{T}^0_0(0, \hat{\boldsymbol{k}})_{\mathrm{M1}}$	1
$\mathcal{T}^1_0(0, \hat{\boldsymbol{k}})_{\mathrm{M1}}$	0
$\mathcal{T}^1_1(0, \hat{\boldsymbol{k}})_{\mathrm{M1}}$	0
$\mathcal{T}^2_0(0, \hat{\boldsymbol{k}})_{\mathrm{M1}}$	$\frac{1}{2\sqrt{2}}(3\cos^2 \vartheta - 1)$
$\mathcal{T}^2_1(0, \hat{\boldsymbol{k}})_{\mathrm{M1}}$	$-\frac{\sqrt{3}}{2} \sin \vartheta \cos \vartheta \, e^{i\varphi}$
$\mathcal{T}^2_2(0, \hat{\boldsymbol{k}})_{\mathrm{M1}}$	$\frac{\sqrt{3}}{4} \sin^2 \vartheta \, e^{i2\varphi}$
	$\mathcal{T}^K_Q(1, \hat{\boldsymbol{k}})_{\mathrm{M1}}$
$\mathcal{T}^0_0(1, \hat{\boldsymbol{k}})_{\mathrm{M1}}$	0
$\mathcal{T}^1_0(1, \hat{\boldsymbol{k}})_{\mathrm{M1}}$	0
$\mathcal{T}^1_1(1, \hat{\boldsymbol{k}})_{\mathrm{M1}}$	0
$\mathcal{T}^2_0(1, \hat{\boldsymbol{k}})_{\mathrm{M1}}$	$\frac{3}{2\sqrt{2}} \cos 2\gamma \sin^2 \vartheta$
$\mathcal{T}^2_1(1, \hat{\boldsymbol{k}})_{\mathrm{M1}}$	$\frac{\sqrt{3}}{2}(\cos 2\gamma \cos \vartheta + i \sin 2\gamma) \sin \vartheta \, e^{i\varphi}$
$\mathcal{T}^2_2(1, \hat{\boldsymbol{k}})_{\mathrm{M1}}$	$\frac{\sqrt{3}}{4}[\cos 2\gamma(1 + \cos^2 \vartheta) + i2 \sin 2\gamma \cos \vartheta]e^{i2\varphi}$
	$\mathcal{T}^K_Q(2, \hat{\boldsymbol{k}})_{\mathrm{M1}}$
$\mathcal{T}^0_0(2, \hat{\boldsymbol{k}})_{\mathrm{M1}}$	0
$\mathcal{T}^1_0(2, \hat{\boldsymbol{k}})_{\mathrm{M1}}$	0
$\mathcal{T}^1_1(2, \hat{\boldsymbol{k}})_{\mathrm{M1}}$	0
$\mathcal{T}^2_0(2, \hat{\boldsymbol{k}})_{\mathrm{M1}}$	$-\frac{3}{2\sqrt{2}} \sin 2\gamma \sin^2 \vartheta$
$\mathcal{T}^2_1(2, \hat{\boldsymbol{k}})_{\mathrm{M1}}$	$-\frac{\sqrt{3}}{2}(\sin 2\gamma \cos \vartheta - i \cos 2\gamma) \sin \vartheta \, e^{i\varphi}$
$\mathcal{T}^2_2(2, \hat{\boldsymbol{k}})_{\mathrm{M1}}$	$-\frac{\sqrt{3}}{4}[\sin 2\gamma(1 + \cos^2 \vartheta) - i2 \cos 2\gamma \cos \vartheta]e^{i2\varphi}$
	$\mathcal{T}^K_Q(3, \hat{\boldsymbol{k}})_{\mathrm{M1}}$
$\mathcal{T}^0_0(3, \hat{\boldsymbol{k}})_{\mathrm{M1}}$	0
$\mathcal{T}^1_0(3, \hat{\boldsymbol{k}})_{\mathrm{M1}}$	$\frac{\sqrt{3}}{2} \cos \vartheta$
$\mathcal{T}^1_1(3, \hat{\boldsymbol{k}})_{\mathrm{M1}}$	$-\frac{\sqrt{3}}{2} \sin \vartheta \, e^{i\varphi}$
$\mathcal{T}^2_0(3, \hat{\boldsymbol{k}})_{\mathrm{M1}}$	0
$\mathcal{T}^2_1(3, \hat{\boldsymbol{k}})_{\mathrm{M1}}$	0
$\mathcal{T}^2_2(3, \hat{\boldsymbol{k}})_{\mathrm{M1}}$	0

NOTE.—The components with negative Q value can be obtained from the conjugation property, $\mathcal{T}^K_{-Q}(i, \hat{\boldsymbol{k}})_{\mathrm{M1}} = (-1)^Q[\mathcal{T}^K_Q(i, \hat{\boldsymbol{k}})_{\mathrm{M1}}]^*$. The angular parameters for the observer's geometry, ϑ, φ, and γ, are defined in Fig. 1.

2.2. *The No-Coherence Hypothesis*

In writing equation (1) we in principle allowed for the presence of quantum coherences between different Zeeman sublevels $(\alpha_0 JM)$ of the excited level, since we did not impose any restrictions on the Q components of the statistical tensor. It is therefore appropriate to state at this point the general properties of the radiating atom, concerning quantum coherences between atomic levels, in light of the different processes involved in the excitation and de-excitation of those levels.

First of all, quantum coherences between different J levels can always be neglected in our problem. This is easily understood when the J levels pertain to the same term α, because the fine-structure splitting is much larger than the typical Zeeman splitting for the ionic species of interest and for the range of magnetic intensities that are believed to exist in the corona (except perhaps for Rydberg states of the ion), so the quantum states associated with those levels evolve incoherently. When J levels from different atomic terms are involved, instead, such a conclusion is less obvious, as level crossing in principle can occur because of distinct terms that overlap in energy range. However, for the ionic species of interest, this kind of level crossing never involves the ground term, whereas higher terms are populated and depopulated only by isotropic collisional and radiative processes (see § 3), so that all J levels above the ground term are always in a condition of natural excitation (cf. Sahal-Bréchot 1977), meaning that the magnetic substates are equally and incoherently populated within a given level (αJ). For all these reasons, it is safe to assume that quantum coherences between any J levels in the atom can be neglected. This assumption is ultimately expressed by the condition of block-diagonality of the density matrix in standard representation with respect to α and J,

$$\rho(\alpha JM, \alpha' J' M') = \delta_{\alpha\alpha'} \delta_{JJ'} \rho_{\alpha J}(M, M') . \tag{8}$$

For the same reason, all Zeeman sublevels above the ground term also are in a condition of natural excitation. In addition, all lines of interest form in the "strong-field" regime, such that $\omega_L \gg A_{M1}$, where ω_L is the Larmor frequency of the applied magnetic field and A_{M1} the Einstein coefficient for the spontaneous M1 transition of interest. Therefore, quantum coherences between any Zeeman sublevels in the atom can also be neglected in the B frame, so we can write, in general,

$$\rho_{\alpha J}(M, M') = \delta_{MM'} \rho_{\alpha J}(M, M) . \tag{9}$$

As we already observed, in the formalism of the irreducible spherical tensors, condition (9) translates into

$$\rho^K_Q(\alpha J) = \delta_{Q0} \rho^K_0(\alpha J) . \tag{10}$$

In that case equation (1) becomes more simply

$$\varepsilon_i(\omega, \hat{\boldsymbol{k}}) = \frac{\hbar\omega}{4\pi} \mathcal{N}(2J+1) A(\alpha_0 J \to \alpha_0 J_0)_{M1} \sum_{KK'} \sqrt{3(2K+1)(2K'+1)} \rho^K_0(\alpha_0 J) \mathcal{T}^{K'}_0(i, \hat{\boldsymbol{k}})_{M1}$$
$$\times \sum_{MM_0, q} (-1)^{J-M_0-1} \phi(\omega_{\alpha_0 JM, \alpha_0 J_0 M_0} - \omega) \begin{pmatrix} J & J & K \\ M & -M & 0 \end{pmatrix} \begin{pmatrix} J & J_0 & 1 \\ -M & M_0 & q \end{pmatrix}^2 \begin{pmatrix} 1 & 1 & K' \\ -q & q & 0 \end{pmatrix} . \tag{11}$$

2.3. *First-Order Expansion of the Emission Coefficients*

Because of the high temperatures and low densities in the corona, the Voigt broadening profile, ϕ, that enters equation (11) is Doppler dominated, and the typical line width for the lines and magnetic intensities of interest is much larger (by at least 2–3 orders of magnitude) than the typical Zeeman splitting. In this situation, it is safe to approximate the profile ϕ in equation (11) by its Taylor expansion in terms of the Zeeman splitting, $\delta\omega_{MM_0}$, about the center of gravity of the line, $\bar{\omega} \equiv \omega_{\alpha_0 J, \alpha_0 J_0}$. Limiting this expansion to the first order of $\delta\omega_{MM_0}$, we then have

$$\phi(\omega_{\alpha_0 JM, \alpha_0 J_0 M_0} - \omega) = \phi(\bar{\omega} - \omega) + \phi'(\bar{\omega} - \omega) \delta\omega_{MM_0} , \tag{12}$$

where the Zeeman splitting is, to the first order of perturbation,

$$\delta\omega_{MM_0} = \omega_L (g_{\alpha_0 J} M - g_{\alpha_0 J_0} M_0) , \tag{13}$$

$g_{\alpha_0 J}$ and $g_{\alpha_0 J_0}$ being the Landé factors of the levels $(\alpha_0 J)$ and $(\alpha_0 J_0)$, respectively. Substitution of equations (12) and (13) into equation (11) then yields, after summation over the magnetic quantum numbers through standard methods of Racah's algebra, the emission coefficients for the scattered radiation as the sum of a zeroth-order contribution and a first-order contribution,

$$\varepsilon_i(\omega, \hat{\boldsymbol{k}}) = \varepsilon^{(0)}_i(\omega, \hat{\boldsymbol{k}}) + \varepsilon^{(1)}_i(\omega, \hat{\boldsymbol{k}}) .$$

The expression of $\varepsilon^{(0)}_i(\omega, \hat{\boldsymbol{k}})$ is derived simply by means of a summation formula for the product of four 3-j symbols (e.g., eq. [8], p. 454, of Varshalovich, Moskalev, & Khersonskii 1988). One then finds (see also LA84, eq. [33], with $Q = 0$)

$$\varepsilon^{(0)}_i(\omega, \hat{\boldsymbol{k}}) = \frac{\hbar\omega}{4\pi} \mathcal{N}(2J+1) A(\alpha_0 J \to \alpha_0 J_0)_{M1} \phi(\bar{\omega} - \omega) \sum_K (-1)^{1+J+J_0} \sqrt{3} \begin{Bmatrix} 1 & 1 & K \\ J & J & J_0 \end{Bmatrix} \rho^K_0(\alpha_0 J) \mathcal{T}^K_0(i, \hat{\boldsymbol{k}})_{M1} . \tag{14}$$

The derivation of $\varepsilon^{(1)}_i(\omega, \hat{\boldsymbol{k}})$ is only slightly more involved. First one has to express the azimuthal quantum numbers M and M_0 from equation (13) in terms of 3-j symbols, through the formula

$$m = (-1)^{j-m} \sqrt{j(j+1)(2j+1)} \begin{pmatrix} j & j & 1 \\ m & -m & 0 \end{pmatrix} , \tag{15}$$

and then to perform the two resulting sums of products of five 3-j symbols by means of appropriate formulae (e.g., eqs. [13] and [14], p. 456, of Varshalovich et al. 1988). One then finds

$$\varepsilon_i^{(1)}(\omega, \hat{\boldsymbol{k}}) = \omega_L \frac{\hbar\omega}{4\pi} \mathcal{N}(2J+1) A(\alpha_0 J \rightarrow \alpha_0 J_0)_{M1} \phi'(\bar{\omega}-\omega) \sum_{KK'} \sqrt{3(2K+1)(2K'+1)} \begin{pmatrix} 1 & K & K' \\ 0 & 0 & 0 \end{pmatrix}$$

$$\times \left[(-1)^{J-J_0-1} g_{\alpha_0 J} \sqrt{J(J+1)(2J+1)} \begin{Bmatrix} 1 & K & K' \\ J & J & J \end{Bmatrix} \begin{Bmatrix} 1 & 1 & K' \\ J & J & J_0 \end{Bmatrix} \right.$$

$$\left. + g_{\alpha_0 J_0} \sqrt{J_0(J_0+1)(2J_0+1)} \begin{Bmatrix} 1 & K & K' \\ J_0 & J & 1 \end{Bmatrix} \right] \rho_0^K(\alpha_0 J) \mathcal{T}_0^{K'}(i, \hat{\boldsymbol{k}})_{M1} \, . \tag{16}$$

We note that in equations (14) and (16), 6-j and 9-j symbols (see, e.g., Brink & Satchler 1968) are obtained as a consequence of the contraction of the 3-j symbols of the original expression, equation (11).

By comparison of equations (14) and (16), we see at once that the magnitude of the first-order contribution to the scattered radiation is of the order of $\omega_L(\phi'/\phi) \sim \omega_L/\Delta\omega_D$ times the zeroth-order contribution. Therefore, given the magnetic intensity and coronal temperature, the first-order contribution is larger the smaller the frequency of the M1 transition under investigation. For this reason, M1 coronal lines in the infrared are to be preferred over visible lines for detection of circular polarization induced by the weak coronal magnetic fields. This fact also provides further justification for the neglect of circular polarization in earlier theoretical treatments of M1 coronal line formation, since high-quality spectropolarimetry in the infrared has only recently become possible (Kuhn 1995).

The irreducible representation adopted for equations (14) and (16) provides a direct physical interpretation of the contribution of different multipole orders of the density matrix, describing different conditions of atomic polarization, to the polarization signature of the scattered radiation. First of all, from the 6-j symbol in equation (14), we see that only the multipole orders $K = 0$ (level population; see eq. [3]), $K = 1$ (level orientation; see eq. [4]), and $K = 2$ (level alignment; see eq. [5]), can contribute to the zeroth-order emission coefficients of the scattered radiation, whereas in equation (16) a contribution from $K = 3$ can also be present (for $K' = 2$; see 3-j symbol in eq. [16]). From inspection of equations (14) and (16) and Table 1, we then can write the correspondences in Table 2.

This has to be read in the sense that, for each value of i, only the corresponding values of K listed in the table can contribute to the ith component of the emission vector to each respective order in $\omega_L/\Delta\omega_D$. This table illustrates the well-known result that, to zeroth order in the Taylor expansion of the line profile, linear polarization in the scattered radiation ($i = 1,2$) can be produced only in the presence of atomic alignment ($K = 2$), whereas atomic orientation ($K = 1$) is needed in order to produce circular polarization ($i = 3$). In the next section we will see that atomic orientation can safely be neglected in the solar corona, because the radiation field from the underlying photosphere is, to a very good approximation, unpolarized. In that case, Table 2 shows additionally that the lowest order of circular polarization in the scattered radiation is determined by the (longitudinal) Zeeman effect ($K = 0$), rather than by atomic alignment as in the case of linear polarization. This justifies mathematically the fact, mentioned in § 1, that circular polarization could be neglected in earlier work on the theory of M1 coronal-line formation (e.g., Sahal-Bréchot 1974, 1977; House 1977), because these magnetic, first-order effects were undetectable with the instrumentation available at that time but should be within reach of the present spectropolarimetric techniques and instrumentation (e.g., Kuhn 1995). Finally, from Table 2 we also see that there is no contribution from atomic population ($K = 0$) to linear polarization ($i = 1,2$). As in the case of circular polarization, such a contribution is associated with the (transverse) Zeeman effect, and it would appear in the expressions of the emission coefficients only if we expanded the line broadening profile, ϕ, to second order in the Zeeman splittings (cf. eqs. [12] and [13]). These magnetic, second-order effects on linear polarization are completely undetectable for the magnetic flux densities characteristic of the solar corona, so they are not considered here.

2.4. *Choice of the Frame of Reference*

We recall that equations (14) and (16) express the emission coefficients in the B frame. As originally pointed out by Charvin (1965), this is the proper frame for magnetic-field diagnostics, because the scattered radiation is most simply expressed in terms of the inclination angle of the magnetic field on the LOS and of the position angle of the magnetic-field projection onto the POS. In our derivation, that "simplicity" is implied by the fact that only the components with $Q = 0$ of the geometric

TABLE 2

CONTRIBUTING MULTIPLES OF THE DENSITY MATRIX

i	$\varepsilon_i^{(0)}(\omega, \hat{\boldsymbol{k}})$	$\varepsilon_i^{(1)}(\omega, \hat{\boldsymbol{k}})$
0	0, 2	1, 3
1	2	1, 3
2	2	1, 3
3	1	0, 2

tensors $\mathcal{T}^K_Q(i, \hat{\boldsymbol{k}})_{\rm M1}$ enter the emission coefficients in the B frame (see Table 1) and therefore it is ultimately related to the no-coherence hypothesis (§ 2.2).

In forward modeling, instead, it is more convenient to express the emission coefficients for the scattered radiation, equations (14) and (16), in a frame of reference with the x_3-axis directed as the local vertical of the Sun at the observed point (the "S frame"), making use of the transformation property of the geometric tensors under rotation of the coordinate system, equation (7b). We then have

$$\mathcal{T}^K_0(i, \hat{\boldsymbol{k}})_{\rm M1} = \sum_Q \mathcal{D}^K_{Q0}(R)[\mathcal{T}^K_Q(i, \hat{\boldsymbol{k}})_{\rm M1}]_S \,, \tag{17}$$

where R is the quantum operator corresponding to the Eulerian rotation that transforms the S frame into the B frame. If the x_3-axis of the B frame has the direction (ϑ_B, φ_B) in the S frame (see Fig. 5), we can choose the Eulerian rotation so that the operator R has the form

$$R(\varphi_B, \vartheta_B, 0) = \exp(-i\varphi_B J_3) \exp(-i\vartheta_B J_2) \,,$$

with J_i ($i = 1, 2, 3$) being the Cartesian components of the total angular momentum operator, $\boldsymbol{J}$, in the S frame. The rotation matrix entering equation (17) is then explicitly given by

$$\mathcal{D}^K_{Q0}(R) = \exp(-i\varphi_B Q) d^K_{Q0}(\vartheta_B) \,. \tag{18}$$

[For $K \leq 2$, the real quantities $d^K_{QQ'}(\vartheta)$ are conveniently tabulated by Brink & Satchler 1968, in the form of algebraic functions of ϑ.] The explicit expressions of the emission coefficients as functions of the different diagnostic quantities in both the B and S frames will be given in § 4.

It is important to observe that, although both $\mathcal{D}^K_{Q0}(R)$ and $[\mathcal{T}^K_Q(i, \hat{\boldsymbol{k}})_{\rm M1}]_S$ are in general complex quantities, the sum over Q in equation (17) is a real quantity. In fact, because of the conjugation properties of the rotation matrices $\mathcal{D}^K_{QQ'}(R)$ (e.g., Brink & Satchler 1968) and of the geometric tensors $\mathcal{T}^K_Q(i, \hat{\boldsymbol{k}})_{\rm M1}$ (see Table 1),

$$[\mathcal{D}^K_{QQ'}(R)]^* = (-1)^{Q-Q'} \mathcal{D}^K_{-Q-Q'}(R) \,, \qquad [\mathcal{T}^K_Q(i, \hat{\boldsymbol{k}})_{\rm M1}]^* = (-1)^Q \mathcal{T}^K_{-Q}(i, \hat{\boldsymbol{k}})_{\rm M1} \,,$$

we have

$$\begin{aligned}\sum_Q [\mathcal{D}^K_{Q0}(R)]^* [\mathcal{T}^K_Q(i, \hat{\boldsymbol{k}})_{\rm M1}]^*_S &= \sum_Q (-1)^{2Q} \mathcal{D}^K_{-Q0}(R)[\mathcal{T}^K_{-Q}(i, \hat{\boldsymbol{k}})_{\rm M1}]_S \\ &= \sum_{Q'} \mathcal{D}^K_{Q'0}(R)[\mathcal{T}^K_{Q'}(i, \hat{\boldsymbol{k}})_{\rm M1}]_S \,.\end{aligned}$$

In particular, this argument shows that $\mathcal{T}^K_0(i, \hat{\boldsymbol{k}})_{\rm M1}$, $K = 0,1,2$, are real quantities in any frame of reference (see Table 1).

3. STATISTICAL-EQUILIBRIUM EQUATIONS

Equations (14) and (16) give the Stokes vector of the scattered radiation, once the statistical-tensor components for the initial level of the transition, $\rho^K_0(\alpha_0 J)$, have been determined by solving the set of statistical-equilibrium equations for the radiating atom. These equations form a set of first-order, linear ordinary differential equations, whose solution in the stationary regime completely determines the populations of the atomic substates. (Because the coronal plasma is optically thin, we can neglect any "back-reaction" of the emitted radiation on the statistical equilibrium of the atom.) If only radiative processes are included, the statistical-equilibrium equations for our problem have the form (cf. LA84, eq. [47])

$$\frac{d}{dt}\rho^K_0(\alpha J) = -R^{(1)}_{K0}(\alpha J) - R^{(2)}_{K0}(\alpha J) + R^{(3)}_{K0}(\alpha J) + R^{(4)}_{K0}(\alpha J) + R^{(5)}_{K0}(\alpha J) - R^{(6)}_{K0}(\alpha J) \,, \tag{19}$$

where $R^{(i)}$ are the radiative rates for the different processes depicted in Figure 2. We notice that we accounted for stimulated-emission processes (rates $R^{(2)}$ and $R^{(5)}$), because in the case of infrared lines (approximately for wavelengths $\gtrsim 2$ μm) such processes can compete with spontaneous-emission processes in determining the population and polarization of the atomic levels. (On the contrary, for spectral lines in the visible, stimulated emission can always be safely neglected.) One should also notice that in equation (19) the complex term that is responsible for the phenomenon of "relaxation of coherences" in the Hanle-effect regime of magnetic fields (see, e.g., LA85, eq. [11]) is absent because of our initial assumption of vanishing coherences between different Zeeman substates, equations (8) and (9). For this reason, in the absence of coherences, the magnetic field can affect the density-matrix elements of the atomic system only through a modification of the radiative rates $R^{(i)}$ (see later in this section).

Besides radiative processes, collisional excitation and de-excitation (induced by inelastic and superelastic collisions, respectively) are also important for these lines. In the usually adopted impact approximation (the collision time assumed to be much smaller than the lifetimes of the levels), the associated collisional rates, $C^{(2)}$, $C^{(3)}$, $C^{(5)}$, and $C^{(6)}$, can simply be added to the corresponding radiative rates (e.g., Lamb & ter Haar 1971). Collision-induced transitions between different Zeeman sublevels within the same level (αJ) must also be taken into account. These so-called depolarizing, collisional transitions contribute an additional collisional rate, $C^{(0)}$, to the statistical-equilibrium equations.

The multilevel problem underlying the formation of the investigated lines, along with the kind of processes involved in the excitation and de-excitation of the levels, is sketched in Figure 3. In general, all six radiative rates for M1 transitions, and all five collisional rates, must be considered for transitions within a given term α (including the ground term). That term is connected to upper and lower terms, α_u and α_l, that are well separated in energy from α (so that stimulated emission can be neglected), through collisional excitation (transition rates $C^{(3)}$ and $C^{(6)}$), and through either E1 spontaneous de-excitation (transition rates $R^{(1)}$ and $R^{(4)}$ for E1 transitions) or M1 spontaneous de-excitation plus collisional de-excitation (transition

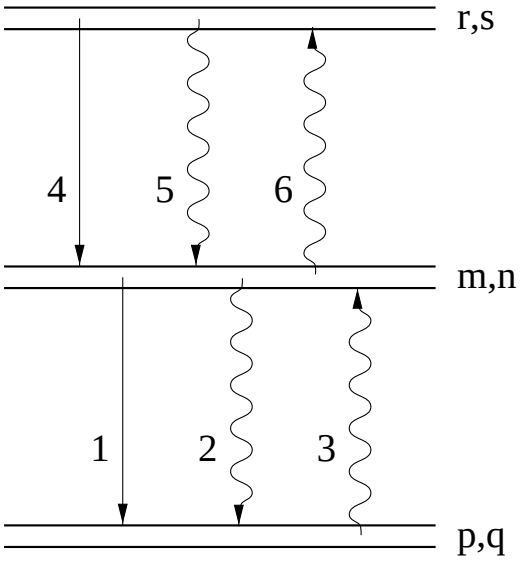

FIG. 2.—Grotrian diagram for the radiative excitation and de-excitation processes affecting the density-matrix elements of the sublevels m and n. Straight lines represent spontaneous emission processes, whereas wavy lines represent radiation-field–induced processes (i.e., absorption and stimulated emission).

rates $R^{(1)}$ and $R^{(4)}$ for M1 transition plus $C^{(2)}$ and $C^{(5)}$). However, if two different terms, α and α', are very close or even overlap in energy, radiative (besides collisional) excitation between the two terms becomes possible, so that all six radiative rates (for E1 and M1 transitions) need be included in the multilevel calculation. In the case of overlapping terms, level crossing can also become an issue, since stimulated emission can in principle create coherences between the crossing levels. However, for all ions of interest, even in the presence of kilogauss magnetic fields, level crossing involves only highly excited levels that rapidly decay via spontaneous de-excitation, so those levels are always naturally populated. For the same reason, J can be considered a "good quantum number" for the description of the multilevel atom, even in the presence of the coronal magnetic field.

Taking into account collisions, equation (19) becomes

$$\frac{d}{dt}\rho^K_0(\alpha J) = -R^{(1)}_{K0}(\alpha J) - R^{(2)}_{K0}(\alpha J) + R^{(3)}_{K0}(\alpha J) + R^{(4)}_{K0}(\alpha J) + R^{(5)}_{K0}(\alpha J) - R^{(6)}_{K0}(\alpha J)$$
$$- C^{(0)}_{K0}(\alpha J) - C^{(2)}_{K0}(\alpha J) + C^{(3)}_{K0}(\alpha J) + C^{(5)}_{K0}(\alpha J) - C^{(6)}_{K0}(\alpha J)\ . \quad (20)$$

Because we are assuming completely isotropic collisions, the various collisional transition rates, $C^{(i)}$, relate, in each statistical-equilibrium equation, only statistical-tensor components with the same multipole order K. In other words, in equation (20)

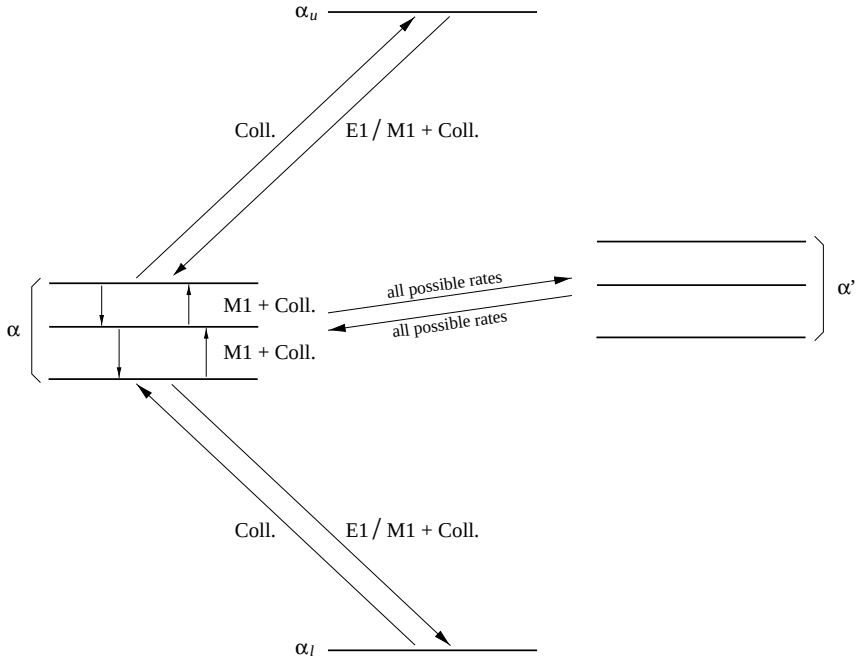

FIG. 3.—Simplified scheme of the multilevel problem for the coronal forbidden lines of interest. α represents the general term of the atom, whereas α_u and α_l are representative of upper and lower terms that are well separated in energy from α. α' is representative of possible terms that overlap in energy with the given term α. Zeeman sublevels are not resolved in this picture.

the collisional transition rates will involve only statistical-tensor components of the form $\rho^K_0(\alpha' J')$. (This is a general property of the transition rates expressed in the representation of the irreducible spherical tensors, when only isotropic processes are active. In particular, that property would hold as well for the radiative rates in case of a completely isotropic incident radiation field; cf. eqs. [24b], [24c], [24e], and [24f] below, with the restriction $K'' = 0$.) As we anticipated in § 1, we do not further discuss the problem of collisions here and defer it to future work in progress in which specific lines of interest will be considered.

We should notice that ionization and recombination rates are not included in equation (20), as these rates are much smaller than the radiative and collisional rates associated with transitions within a given ionic species, under conditions close to ionization equilibrium. For these reasons, the statistical-equilibrium equation (20) refers to only the specific ion undergoing the transition associated with the particular coronal line under investigation.

The solution of the set of statistical-equilibrium equations (20) in the stationary regime is finally determined by equating to zero the time-derivative term on the left-hand side, so that a homogeneous set of linear equations with null determinant is obtained. As is customary, one of the redundant equations is replaced by the normalization condition for the trace of the statistical operator of the atom (cf. eq. [3],

$$\mathrm{Tr}(\rho) = \sum_{\alpha J} \sqrt{2J+1}\, \rho^0_0(\alpha J) = 1 \,, \tag{21}$$

which expresses the conservation of number density for the specific ion of interest.

3.1. *Hypotheses on the Incident Radiation Field*

We now introduce two assumptions on the nature of the incident radiation field from the photosphere that will simplify considerably the calculation of the radiative rates associated with radiation-field–induced processes (see Fig. 2). The selective "population" and "depopulation" of a given multipole K_0 of the statistical tensor by radiation-field–induced processes at the frequency ω_0 is determined, via particular selection rules for the multipole orders (see eqs. [24b], [24c], [24e], and [24f], below), by the following tensors of the average incident radiation field,

$$\bar{J}^K_Q(\omega_0)_{\mathrm{E1,M1}} = \int d\omega\, \phi(\omega_0 - \omega) \oint \frac{d\hat{\boldsymbol{k}}}{4\pi} \sum_{i=0}^{3} \mathscr{T}^K_Q(i, \hat{\boldsymbol{k}})_{\mathrm{E1,M1}}\, S_i(\omega, \hat{\boldsymbol{k}}) \,, \tag{22a}$$

$$\bar{F}^K_Q(\omega_0)_{\mathrm{E1,M1}} = \bar{J}^K_Q(\omega_0)_{\mathrm{E1,M1}}\{\phi \to \psi\} \,, \tag{22b}$$

where $S_i(\omega, \hat{\boldsymbol{k}})$ are the four Stokes parameters of the incident radiation field. The first assumption we make is that the incident radiation field is, to a very good approximation, unpolarized, so we can put $S_i(\omega, \hat{\boldsymbol{k}}) = \delta_{i0}\, S_0(\omega, \hat{\boldsymbol{k}})$ in equations (22a) and (22b). From Table 1 and equation (6) we then see that $\bar{J}^1_Q(\omega_0)_{\mathrm{E1,M1}} = \bar{F}^1_Q(\omega_0)_{\mathrm{E1,M1}} = 0$ in any frame of reference (see, e.g., eq. [26] below). Second, we assume that the incident radiation from the photosphere is flat over the entire spectral range of the radiative transition at the frequency ω_0 (see § 1.1), so we can additionally write $S_i(\omega, \hat{\boldsymbol{k}}) = \delta_{i0}\, S_0(\omega_0, \hat{\boldsymbol{k}})$. This last assumption is a safe one for the infrared spectral region, but it needs to be carefully checked when dealing with transitions in the visible, where the line density in the photospheric spectrum and line depths are much larger than in the infrared. With these two approximations, and also considering the normalization properties of the profiles ϕ and ψ, equations (22a) and (22b) become more simply

$$(\bar{J}^K_Q)(\omega_0)_{\mathrm{E1,M1}} = \oint \frac{d\hat{\boldsymbol{k}}}{4\pi}\, \mathscr{T}^K_Q(0, \hat{\boldsymbol{k}})_{\mathrm{E1,M1}} S_0(\omega_0, \hat{\boldsymbol{k}}) \,, \tag{23a}$$

$$(\bar{F}^K_Q)(\omega_0)_{\mathrm{E1,M1}} = 0 \,. \tag{23b}$$

3.2. *Irreducible Representation of the Radiative Rates*

Following LA84 (cf. his eqs. [49]–[54]), and taking into account the no-coherence condition (10) and the flat-spectrum approximation, equations (23a) and (23b), we find that the radiative rates governing the statistical equilibrium of the multilevel atom are (the ordering symbols "$\prec$" and "$\succ$" in the following summations determine the energy ordering of the levels)

$$R^{(1)}_{K0}(\alpha J)_{\mathrm{E1,M1}} = \sum_{\alpha' J' \prec \alpha J} A(\alpha J \to \alpha' J')_{\mathrm{E1,M1}}\, \rho^K_0(\alpha J) \,, \tag{24a}$$

$$R^{(2)}_{K0}(\alpha J)_{\mathrm{E1,M1}} = \sum_{\alpha' J' \prec \alpha J} (2J+1) B(\alpha J \to \alpha' J')_{\mathrm{E1,M1}} \sum_{K' K''} (-1)^{J-J'+1} \sqrt{3(2K+1)(2K'+1)(2K''+1)} \times \begin{pmatrix} K & K' & K'' \\ 0 & 0 & 0 \end{pmatrix} \begin{Bmatrix} K & K' & K'' \\ J & J & J \end{Bmatrix} \begin{Bmatrix} 1 & 1 & K'' \\ J & J & J' \end{Bmatrix} \rho^{K'}_0(\alpha J) \bar{J}^{K''}_0(\omega_{\alpha J, \alpha' J'})_{\mathrm{E1,M1}} \,, \tag{24b}$$

$$R^{(3)}_{K0}(\alpha J)_{\mathrm{E1,M1}} = \sum_{\alpha' J' \prec \alpha J} (2J'+1) B(\alpha' J' \to \alpha J)_{\mathrm{E1,M1}} \sum_{K' K''} (-1)^{K'} \sqrt{3(2K+1)(2K'+1)(2K''+1)} \times \begin{pmatrix} K & K' & K'' \\ 0 & 0 & 0 \end{pmatrix} \begin{Bmatrix} K & K' & K'' \\ J & J' & 1 \\ J & J' & 1 \end{Bmatrix} \rho^{K'}_0(\alpha J) \bar{J}^{K''}_0(\omega_{\alpha J, \alpha' J'})_{\mathrm{E1,M1}} \,, \tag{24c}$$

$$R^{(4)}_{K0}(\alpha J)_{\mathrm{E1,M1}} = \sum_{\alpha' J' \succ \alpha J} (2J'+1) A(\alpha' J' \to \alpha J)_{\mathrm{E1,M1}} (-1)^{J+J'+1+K} \begin{Bmatrix} J & J & K \\ J' & J' & 1 \end{Bmatrix} \rho^K_0(\alpha' J') \,, \tag{24d}$$

$$R^{(5)}_{K0}(\alpha J)_{\mathrm{E1,M1}} = \sum_{\alpha' J' \succ \alpha J} (2J'+1) B(\alpha' J' \rightarrow \alpha J)_{\mathrm{E1,M1}} \sum_{K' K''} (-1)^{K'+K''} \sqrt{3(2K+1)(2K'+1)(2K''+1)}$$
$$\times \begin{pmatrix} K & K' & K'' \\ 0 & 0 & 0 \end{pmatrix} \begin{Bmatrix} K & K' & K'' \\ J & J' & 1 \\ J & J' & 1 \end{Bmatrix} \rho^{K'}_0(\alpha J) \bar{J}^{K''}_0(\omega_{\alpha' J, \alpha J'})_{\mathrm{E1,M1}} \tag{24e}$$

$$R^{(6)}_{K0}(\alpha J)_{\mathrm{E1,M1}} = \sum_{\alpha' J' \succ \alpha J} (2J+1) B(\alpha J \rightarrow \alpha' J')_{\mathrm{E1,M1}} \sum_{K' K''} (-1)^{J-J'+1+K+K'} \sqrt{3(2K+1)(2K'+1)(2K''+1)}$$
$$\times \begin{pmatrix} K & K' & K'' \\ 0 & 0 & 0 \end{pmatrix} \begin{Bmatrix} K & K' & K'' \\ J & J & J \end{Bmatrix} \begin{Bmatrix} 1 & 1 & K'' \\ J & J & J' \end{Bmatrix} \rho^{K'}_0(\alpha J) \bar{J}^{K''}_0(\omega_{\alpha' J, \alpha J'})_{\mathrm{E1,M1}} \, . \tag{24f}$$

The various Einstein B coefficients in the previous equations are given by

$$B(\alpha_u J_u \rightarrow \alpha_l J_l)_{\mathrm{E1,M1}} = \frac{4\pi^3 c^2}{\hbar \omega^3_{\alpha_u J_u, \alpha_l J_l}} A(\alpha_u J_u \rightarrow \alpha_l J_l)_{\mathrm{E1,M1}} \, , \tag{25a}$$

$$B(\alpha_l J_l \rightarrow \alpha_u J_u)_{\mathrm{E1,M1}} = \frac{2J_u + 1}{2J_l + 1} B(\alpha_u J_u \rightarrow \alpha_l J_l)_{\mathrm{E1,M1}} \, , \tag{25b}$$

where the ordering of the levels is such that $\alpha_u J_u \succ \alpha_l J_l$. Of course, the radiative rates corresponding to transitions within a given term α are also included in equations (24a)–(24f) for $\alpha' = \alpha$.

We notice that the common 3-j symbol that appears in the expressions of the radiative rates $R^{(2)}$, $R^{(3)}$, $R^{(5)}$, and $R^{(6)}$ implies that $K + K' + K''$ must be an even number. Therefore, it is evident that odd multipole orders of the density matrix (including atomic orientation) cannot be generated from a state of natural excitation of the atom, unless the incident radiation field is circularly polarized [$(\bar{J}^1_Q)_{\mathrm{E1,M1}} \neq 0$]. Analogously, even multipole orders of the density matrix (including atomic alignment) are generated because of the anisotropy of the incident radiation field [$(\bar{J}^2_Q)_{\mathrm{E1,M1}} \neq 0$; see eq. (30b) below]. The presence of isotropic collisions does not change the substance of these conclusions. However, the degree of atomic polarization of a given level (αJ), described by the ratios $\rho^K_0(\alpha J)/\rho^0_0(\alpha J)$, is determined by the relative importance between the radiative and collisional transition rates that contribute to the population of that level, and it is always lower than in the absence of collisions.

3.3. *Magnetic Dependence of the Radiative Rates*

It must be noticed that equations (24a)–(24f) contain no information on the Zeeman patterns of the transitions that contribute to the radiative rates $R^{(i)}$, so the statistical equilibrium of the atom is insensitive to the magnetic-field strength. This results essentially from the flatness of the incident radiation field over a frequency interval much larger than the transition's spectral range. If this assumption were not applicable—in particular, if the spectral details of the incident radiation field were of the order of the Zeeman splitting—the magnetic-field strength would play a role in the radiative rates associated with radiation-field–induced processes, $R^{(2)}$, $R^{(3)}$, $R^{(5)}$, and $R^{(6)}$. (This can easily be seen, for instance, by replacing the profiles ϕ and ψ in eqs. [22a] and [22b] by their first-order Taylor expansions analogous to eq. [12].) However, in that case the hypothesis of complete redistribution would not apply.

Although the statistical equilibrium of the atom is independent of the magnetic-field strength, it is nonetheless sensitive to the direction of the magnetic field. In fact, such dependence enters the radiative rates associated with radiation-field–induced processes through the tensor components of the incident radiation field, $(\bar{J}^K_0)_{\mathrm{E1,M1}}$, which are expressed in the B frame. On the other hand, the incident radiation field from the photosphere takes a simpler form in the S frame defined previously, since it is assumed that the incident radiation field possess cylindrical symmetry about the local vertical of the Sun at the observed point. This symmetry property requires that in the S frame

$$[(\bar{J}^K_Q)_{\mathrm{E1,M1}}]_S = \delta_{Q0} [(\bar{J}^K_0)_{\mathrm{E1,M1}}]_S \, .$$

[To see this, one can consider a frame of reference S' obtained from the S frame through a simple rotation of angle φ about the common x_3-axis of the two frames. Equation (7b) then reduces to $(\mathcal{T}^K_Q)_{S'} = \exp(-i\varphi Q)(\mathcal{T}^K_Q)_S$. If there is cylindrical symmetry about the x_3-axis, then the frames S and S' are undistinguishable, so $(\mathcal{T}^K_Q)_{S'} = (\mathcal{T}^K_Q)_S$. Since φ is arbitrary, the last identity can be satisfied only for $Q = 0$.]

By analogy to equation (17), the tensor components of the incident radiation field in the B frame entering equations (24a) to (24f) are related to those in the S frame by the expression

$$(\bar{J}^K_0)_{\mathrm{E1,M1}} = \sum_Q \mathcal{D}^K_{Q0}(R) [(\bar{J}^K_Q)_{\mathrm{E1,M1}}]_S$$
$$= \mathcal{D}^K_{00}(R) [(\bar{J}^K_0)_{\mathrm{E1,M1}}]_S \, . \tag{26}$$

The rotation matrices $\mathcal{D}^K_{00}(R)$, for $K = 0,1,2$, are now real quantities (cf. eq. [18]) given by

$$d^0_{00}(\vartheta_B) = 1 \, , \tag{27a}$$

$$d^1_{00}(\vartheta_B) = \cos \vartheta_B \, , \tag{27b}$$

$$d^2_{00}(\vartheta_B) = \frac{1}{2}(3\cos^2 \vartheta_B - 1) \, . \tag{27c}$$

Equation (26), together with equations (27a)–(27c), must then be substituted into the rates $R^{(i)}$ in order to express the statistical-equilibrium equations in terms of the tensors of the incident radiation field in the S frame, and the quantity $d^2_{00}(\vartheta_B)$

then is responsible for the dependence on the direction of the magnetic field of the radiative rates associated with radiation-field–induced processes. (Because of the assumption of unpolarized incident radiation field, the sum over K'' implied by those rates is restricted to the values $K'' = 0,2$ only.) In particular, from equations (26) and (27c), we see at once that for $\cos^2 \vartheta_B = 1/3$ (i.e., when ϑ_B is equal to the van Vleck angle $\vartheta_V \approx 54.^\circ 74$), the tensor component $(\bar{J}^2_0)_{E1,M1}$ of the incident radiation field vanishes identically (see also eq. [30b] below). In that case, the atomic system becomes insensitive to the anisotropy of the radiation field, and atomic alignment cannot be produced. Table 2 then illustrates the well-known result that the linear polarization of the scattered radiation must vanish, to first order in the Taylor expansion of the line profile, for this particular configuration of the magnetic field (e.g., Sahal-Bréchot 1974; House 1977; LA85).

The quantities $[(\bar{J}^K_0)_{E1,M1}]_S$ can be calculated through equation (23a), once the geometric tensors $\mathscr{T}^K_Q(i, \hat{k})_{E1,M1}$ have been expressed in the S frame and the intensity $S_0(\hat{k})$ of the incident radiation field from the photosphere has been specified, i.e., once the limb-darkening function, $S_0(\mu)/S_0(0)$ (with $\mu = \cos \zeta$, where ζ is the emergence angle of the incident radiation field; see Fig. 4) has been given for the spectral region of interest (e.g., Allen 1973). If h denotes the height of the observed point above the limb, ϑ_M the semiaperture of the cone of incident radiation from the photosphere at that point, and $R_\odot$ the (average) solar radius, for a given incident direction $\hat{k} \equiv (\vartheta, \varphi)$ referred to the S frame, we have (see Fig. 4)

$$S_0(\hat{k}) = S_0[\mu(\vartheta)] , \tag{28}$$

$$\mu(\vartheta) = \left(1 - \frac{\sin^2 \vartheta}{\sin^2 \vartheta_M}\right)^{1/2} , \qquad \sin \vartheta_M = \left(1 + \frac{h}{R_\odot}\right)^{-1} , \tag{29}$$

where in equation (28) we explicitly made use of the hypothesis of cylindrical symmetry of $S_0(\hat{k})$ in the S frame. We then have, in equations (24b), (24c), (24e), and (24f) (i.e., in the B frame), also taking into account equations (26) and (27a), (27b), and (27c),

$$\bar{J}^0_0 = \frac{1}{2} \int_0^{\vartheta_M} d\vartheta \sin \vartheta S_0[\mu(\vartheta)] , \tag{30a}$$

$$\bar{J}^2_0 = \frac{1}{8\sqrt{2}} (3 \cos^2 \vartheta_B - 1) \int_0^{\vartheta_M} d\vartheta \sin \vartheta (3 \cos^2 \vartheta - 1) S_0[\mu(\vartheta)] . \tag{30b}$$

We note that in the above equations we were able to drop the subscripts "E1" and "M1" from the quantities $(\bar{J}^K_0)_{E1,M1}$, because in the case of unpolarized incident radiation field those are identical in the two cases of E1 and M1 transitions, as demonstrated by equation (6).

From equations (30a) and (30b), we can easily calculate the anisotropy factor of the incident radiation field in the absence of limb darkening,

$$\frac{\bar{J}^2_0}{\bar{J}^0_0} = \frac{1}{4\sqrt{2}} (3 \cos^2 \vartheta_B - 1)(1 + \cos \vartheta_M) \cos \vartheta_M < \frac{1}{\sqrt{2}} . \tag{31}$$

Taking into account realistic limb-darkening functions at various wavelengths in the visible and near-infrared (e.g., Allen 1973) brings a correction to the previous estimate of the anisotropy factor of only a few percent, the correction being more

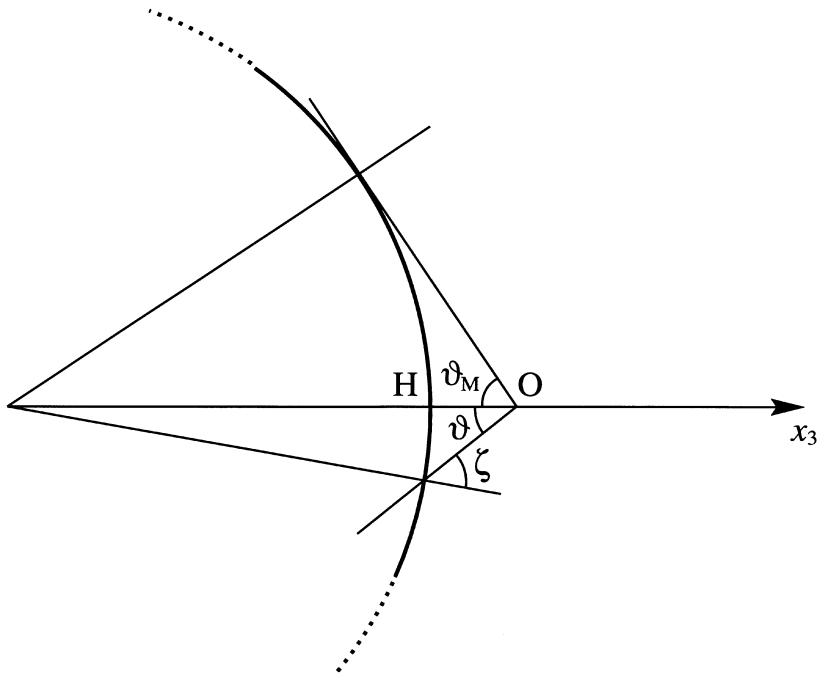

FIG. 4.—Geometry construct for the determination of the radiation field in the S frame. The segment OH = h gives the height of the observed point, O, above the solar surface. The limb-darkening function is given for different emergence angles ζ, in terms of which the polar angle of the incident radiation field in O, $\vartheta \in (0, \vartheta_M)$, can easily be expressed.

important closer to the limb and in the visible. At a distance from the limb $h = 0.5\,R_\odot$, the anisotropy factor can be as large as 46% (for $\vartheta_B = 0$), so the contribution from atomic alignment to the intensity and circular polarization of the scattered radiation can represent an important fraction of the population contribution. This is an important fact to consider in the interpretation of the observed V-polarization signal to estimate the longitudinal magnetic field (see § 4).

4. EXPLICIT FORMULAE FOR THE STOKES PARAMETERS OF THE SCATTERED RADIATION

Once the frequency and the Einstein coefficient for the spontaneous transition $(\alpha_0 J) \rightarrow (\alpha_0 J_0)$ are given and the values of $\rho^K_0(\alpha_0 J)$ (for $K = 0,2$) are derived from the solution of the statistical-equilibrium equation (20), the four Stokes parameters of the scattered radiation can be calculated directly from equations (14) and (16). In this section, the explicit formulae for the four Stokes parameters of the scattered radiation will be derived in order to clarify their dependence on the different diagnostic quantities.

In order to simplify the notation, we introduce the population density of the excited level (see LA84, eq. [43]; see also eq. [3] in this paper),

$$\mathcal{N}_{\alpha_0 J} = \mathcal{N}\sqrt{2J+1}\;\rho^0_0(\alpha_0 J)\,, \tag{32}$$

the "reduced" statistical tensor for that level (see LA84, eq. [39]),

$$\sigma^K_Q(\alpha_0 J) = \frac{\rho^K_Q(\alpha_0 J)}{\rho^0_0(\alpha_0 J)}\,, \tag{33}$$

and the effective Landé factor of the transition $(\alpha_0 J) \rightarrow (\alpha_0 J_0)$ (e.g., Landi Degl'Innocenti 1982),

$$\bar{g}_{\alpha_0 J,\alpha_0 J_0} = \tfrac{1}{2}\,(g_{\alpha_0 J} + g_{\alpha_0 J_0}) + \tfrac{1}{4}\,(g_{\alpha_0 J} - g_{\alpha_0 J_0})[J(J+1) - J_0(J_0+1)]\,. \tag{34}$$

Since the orientation of the atomic system is negligible, we find, after some Racah's algebra,

$$\varepsilon^{(0)}_0(\omega, \hat{\boldsymbol{k}}) = C_{JJ_0}\,\phi(\bar{\omega} - \omega)[1 + D_{JJ_0}\,\sigma^2_0(\alpha_0 J)\mathcal{T}^2_0(0, \hat{\boldsymbol{k}})_{\rm M1}]\,, \tag{35a}$$

$$\varepsilon^{(0)}_i(\omega, \hat{\boldsymbol{k}}) = C_{JJ_0}\,\phi(\bar{\omega} - \omega)D_{JJ_0}\,\sigma^2_0(\alpha_0 J)\mathcal{T}^2_0(i, \hat{\boldsymbol{k}})_{\rm M1}\,, \qquad (i = 1, 2) \tag{35b}$$

$$\varepsilon^{(1)}_3(\omega, \hat{\boldsymbol{k}}) = -\sqrt{\frac{2}{3}}\,\omega_{\rm L}\,C_{JJ_0}\,\phi'(\bar{\omega} - \omega)[\bar{g}_{\alpha_0 J,\alpha_0 J_0} + E_{JJ_0}\,\sigma^2_0(\alpha_0 J)]\mathcal{T}^1_0(3, \hat{\boldsymbol{k}})_{\rm M1}\,, \tag{35c}$$

where[3]

$$C_{JJ_0} = \frac{\hbar\omega}{4\pi}\,\mathcal{N}_{\alpha_0 J}\,A(\alpha_0 J \rightarrow \alpha_0 J_0)_{\rm M1}\,, \tag{36a}$$

$$D_{JJ_0} = (-1)^{1+J+J_0}\sqrt{3(2J+1)}\begin{Bmatrix} 1 & 1 & 2 \\ J & J & J_0 \end{Bmatrix}, \tag{36b}$$

$$E_{JJ_0} = 3\sqrt{2J+1}\left[(-1)^{J-J_0}\,g_{\alpha_0 J}\sqrt{J(J+1)(2J+1)}\begin{Bmatrix} 1 & 2 & 1 \\ J & J & J \end{Bmatrix}\begin{Bmatrix} 1 & 1 & 1 \\ J & J & J_0 \end{Bmatrix}\right.$$

$$\left. - g_{\alpha_0 J_0}\sqrt{J_0(J_0+1)(2J_0+1)}\begin{Bmatrix} 1 & 2 & 1 \\ J_0 & J & 1 \\ J_0 & J & 1 \end{Bmatrix}\right]. \tag{36c}$$

The coefficients D_{JJ_0} and E_{JJ_0} of equations (36b) and (36c) can be given as functions of J or J_0 only, if we explicitly take into account that $|\Delta J| = 1$ for all lines of interest. We then find, for $J = J_0 - 1$ and $J \neq 0$,[4]

$$D_{J,J+1} = \frac{1}{\sqrt{10}}\sqrt{\frac{J(2J-1)}{(J+1)(2J+3)}}\,, \tag{37a}$$

$$E_{J,J+1} = \frac{1}{\sqrt{5}}\sqrt{\frac{(2J-1)(2J+3)}{J(J+1)}}\left[\bar{g}_{\alpha_0 J,\alpha_0 J+1} - g_{\alpha_0 J+1}\,\frac{6J(2J+3) - 12}{(2J+1)(2J+3)}\right], \tag{37b}$$

[3] The coefficient D_{JJ_0} coincides with the symbol $w^{(2)}_{JJ_0}$ introduced in LA84, eq. (38), and conveniently tabulated for all possible transitions $\Delta J = 0, \pm 1$, up to $J = J_0 = 6$. We should also notice that $D_{JJ_0}\,\sigma^2_0(\alpha_0 J)$ is proportional (by a factor $2\sqrt{2}$) to the coefficient η introduced in Sahal-Bréchot 1977, eq. (14).

[4] For $J = 0$, the coefficients D_{JJ_0} and E_{JJ_0} vanish identically, as can be seen directly from eqs. (36b) and (36c). This is as expected, given that the level $J = 0$ cannot be polarized.

whereas, for $J = J_0 + 1$,

$$D_{J_0+1,J_0} = \frac{1}{\sqrt{10}} \sqrt{\frac{(J_0+2)(2J_0+5)}{(J_0+1)(2J_0+1)}}, \tag{38a}$$

$$E_{J_0+1,J_0} = \frac{1}{\sqrt{5}} \sqrt{\frac{(2J_0+1)(2J_0+5)}{(J_0+1)(J_0+2)}} \left(\bar{g}_{\alpha_0 J_0+1,\alpha_0 J_0} - g_{\alpha_0 J_0} \frac{6J_0}{2J_0+1} \right) \tag{38b}$$

From Table 1, the geometric tensors in equations (35a)–(35c) are given by

$$\mathscr{T}^2_0(0, \hat{\boldsymbol{k}})_{\mathrm{M1}} = \frac{1}{2\sqrt{2}} (3 \cos^2 \Theta_B - 1) , \tag{39a}$$

$$\mathscr{T}^2_0(1, \hat{\boldsymbol{k}})_{\mathrm{M1}} = \frac{3}{2\sqrt{2}} \cos 2\gamma_B \sin^2 \Theta_B , \tag{39b}$$

$$\mathscr{T}^2_0(2, \hat{\boldsymbol{k}})_{\mathrm{M1}} = -\frac{3}{2\sqrt{2}} \sin 2\gamma_B \sin^2 \Theta_B , \tag{39c}$$

$$\mathscr{T}^1_0(3, \hat{\boldsymbol{k}})_{\mathrm{M1}} = \sqrt{\frac{3}{2}} \cos \Theta_B , \tag{39d}$$

where we indicated with Θ_B the inclination angle of the magnetic field on the LOS and with γ_B the position angle of the reference direction for linear-polarization measurements in the B frame (see Fig. 5). Therefore, if the reference direction for linear-polarization measurements is set parallel to the projection of the magnetic field onto the POS ($\gamma_B = 0, \pi$), from equations (39b) and (39c), and recalling equation (35b), we see that the U-polarization vanishes, whereas the Q-polarization has the same sign of the "alignment factor," $\sigma^2_0(\alpha_0 J) = \rho^2_0(\alpha_0 J)/\rho^0_0(\alpha_0 J)$. (For E1 transitions, the Q-polarization would show the opposite sign in that case, as suggested by eq. [6]; see also Sahal-Bréchot 1974, eq. [27].) This result was originally derived by Charvin (1965). If the sign of the alignment factor cannot be assessed a priori, the conditions $Q > 0$ and $U = 0$ determine the direction of $\boldsymbol{B}$ in the POS with an ambiguity of 90°.

If the contributions to equations (35a) and (35c) from atomic alignment (i.e., from the terms proportional to D_{JJ_0} and E_{JJ_0} in those equations) are negligible, we easily find that the intensity and the circular-polarization profiles of the scattered

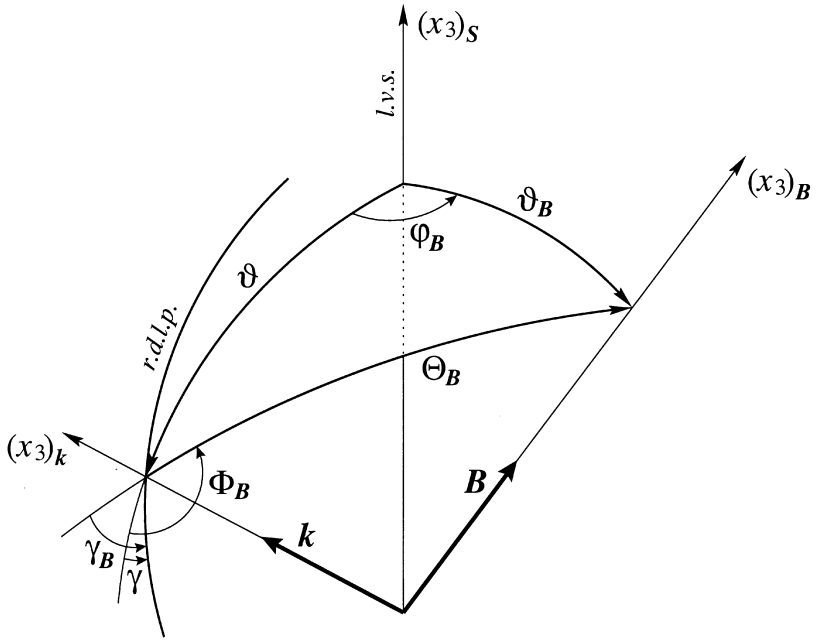

FIG. 5.—Geometry of the magnetic field, $\boldsymbol{B}$, and the propagation vector of the scattered radiation, $\boldsymbol{k}$, relative to the local vertical of the Sun, x_3. Relative geometry of the magnetic field, $\boldsymbol{B}$, the propagation vector of the scattered radiation, $\boldsymbol{k}$, and the local vertical of the Sun at the observed point (*l.v.s.*). The LOS, coincident with $\boldsymbol{k}$, is contained in the $x_1 x_3$ plane of the S frame [which has $x_3 \equiv (x_3)_S$]. The angles ϑ_B and φ_B represent, respectively, the polar and azimuthal angles of the magnetic field in the S frame, whereas Θ_B and Φ_B are the corresponding angles in the frame of reference of the LOS [which has $x_3 \equiv (x_3)_{\boldsymbol{k}}$]. The position angles γ and γ_B determine the reference direction for linear-polarization measurements (*r.d.l.p.*), respectively, in the S frame and in the B frame [which has $x_3 \equiv (x_3)_B$].

radiation are related via the well-known "magnetograph formula,"

$$\varepsilon_3^{(1)}(\omega, \hat{\boldsymbol{k}}) = \bar{g}_{\alpha_0 J, \alpha_0 J_0}\, \omega_{\rm L} \cos \Theta_B \frac{d}{d\omega} \varepsilon_0^{(0)}(\omega, \hat{\boldsymbol{k}}) \,. \tag{40}$$

This property was originally proved by Landi Degl'Innocenti (1982), in the application of resonance scattering in a magnetized plasma to the diagnostics of prominence magnetic fields through the He I D3 line. In that case, in fact, the alignment factor, $\sigma_0^2(\alpha_0 J)$, was only of the order of 10^{-2}, so the correction to equation (40) from atomic alignment could safely be neglected.

In general, from equations (35a) and (35c), we see that equation (40) is modified by the presence of an additional factor

$$\kappa \equiv \frac{1 + E_{JJ_0}\, \sigma_0^2(\alpha_0 J)/\bar{g}_{\alpha_0 J, \alpha_0 J_0}}{1 + [1/(2\sqrt{2})] D_{JJ_0}\, \sigma_0^2(\alpha_0 J)(3\cos^2 \Theta_B - 1)} \,. \tag{41}$$

For the transition $1 \to 0$, the alignment factor can be as large as the anisotropy factor of the incident radiation field (in the approximation of a two-level atom and in the collisionless regime; cf. LA84, eq. [61] and Table 1). In that case, from equations (38a) and (38b), we have $D_{10} = 1$ and $E_{10} = (1/\sqrt{2})\bar{g}_{\alpha_0 1, \alpha_0 0}$, so the deviation from the magnetograph regime of equation (40), as represented by the factor κ, can be important, depending on the inclination angles of the magnetic field on the LOS and on the x_3-axis of the S frame, Θ_B and ϑ_B, respectively, and also on the distance of the observed point from the solar limb, h (cf. eq. [31]). As a typical example, for $\vartheta = 90°$, $(\vartheta_B, \varphi_B) \equiv (30°, 0°)$, and $h = 0.5\, R_\odot$, which give an anisotropy factor of 29%, we find $\kappa \approx 1.23$ for the transition $1 \to 0$, giving a deviation of 23% from the magnetograph regime. For vertical magnetic field, $\vartheta_B = 0°$, and for $h \to \infty$, the anisotropy factor takes its maximum value of $1/\sqrt{2}$. In such a limiting case, and for the same transition $1 \to 0$, the maximum value of $\kappa = 2$ (i.e., a 100% correction to the magnetograph formula) is attained in the limit of vanishing longitudinal fields, $\Theta_B = 90°$.

Note that the contribution from isotropic collisions and cascade processes to the population of the excited level reduces the alignment factor with respect to the maximum possible value that is found in the ideal case of purely radiative excitation from the lower level. Therefore, although the alignment factor is less than unity, it can change substantially depending on the particle density and height in the corona and on the particular line considered, thus complicating the interpretation of the V profile as a diagnostic of field strength in the corona.

Finally, we want to determine expressions for the emission coefficients in the S frame, which is the most convenient if we are interested in the synthesis of Stokes profiles of coronal lines forming within prescribed magnetic-field configurations. As customary, we choose the S frame so that the LOS, $\hat{\boldsymbol{k}}$, is contained in the plane $x_1 x_3$, and we adopt as reference direction for linear-polarization measurements the direction perpendicular to the limb. According to Figure 1, such a choice implies $\varphi = 0$ and $\gamma = 0$, bringing a sensible simplification to the expressions of the geometric tensors in the S frame, $[\mathcal{T}^K_Q(i, \hat{\boldsymbol{k}})_{\rm M1}]_S$.

The components $\mathcal{T}^2_0(0, \hat{\boldsymbol{k}})_{\rm M1}$ and $\mathcal{T}^1_0(3, \hat{\boldsymbol{k}})_{\rm M1}$ of equations (39a) and (39d) are easily expressed in the S frame through the "cosine" formula of spherical trigonometry (see Fig. 5),

$$\cos \Theta_B = \cos \vartheta \cos \vartheta_B + \sin \vartheta \sin \vartheta_B \cos \varphi_B \,. \tag{42}$$

The expressions in the S frame of the components $\mathcal{T}^2_0(1, \hat{\boldsymbol{k}})_{\rm M1}$ and $\mathcal{T}^2_0(2, \hat{\boldsymbol{k}})_{\rm M1}$ of equations (39b) and (39c) are instead more easily determined if we explicitly use the transformation property (17). After some tedious algebra, we find, for Q and U polarizations, respectively,

$$\begin{aligned} \mathcal{T}^2_0(1, \hat{\boldsymbol{k}})_{\rm M1} &= \sum_Q \mathcal{D}^2_{Q0}(R)[\mathcal{T}^2_Q(1, \hat{\boldsymbol{k}})_{\rm M1}]_S \\ &= \frac{3}{\sqrt{2}} \left[\sin^2 \vartheta_B \sin^2 \varphi_B - \frac{1}{2}(1 - \cos^2 \Theta_B) \right], \end{aligned} \tag{43a}$$

$$\begin{aligned} \mathcal{T}^2_0(2, \hat{\boldsymbol{k}})_{\rm M1} &= \sum_Q \mathcal{D}^2_{Q0}(R)[\mathcal{T}^2_Q(2, \hat{\boldsymbol{k}})_{\rm M1}]_S \\ &= \frac{3}{\sqrt{2}} \sin \vartheta_B \sin \varphi_B \sin \Theta_B \cos(\pi - \Phi_B) \,, \end{aligned} \tag{43b}$$

where we indicated with Φ_B the azimuthal angle of $\boldsymbol{B}$ in the frame of reference of the LOS (see Fig. 5; from the figure, we also see that $\gamma = 0$ implies $\gamma_B = \pi - \Phi_B$). In writing equation (43b), we made use of another fundamental formula of spherical trigonometry (see Fig. 5),

$$\sin \Theta_B \cos(\pi - \Phi_B) = \sin \vartheta \cos \vartheta_B - \cos \vartheta \sin \vartheta_B \cos \varphi_B \,. \tag{44}$$

By means of equations (42) and (44), the geometric tensors in the emission coefficients of equations (35a)–(35c) can be expressed as functions of the various angular parameters referred to the particular S frame adopted here.

5. DISCUSSION AND CONCLUSIONS

In this paper we reviewed the theory of formation of optically thin, M1 coronal lines in the presence of magnetic fields. A consistent treatment of all four Stokes parameters, I, Q, U, and V, of the scattered radiation was provided, extending previous work from different authors on this problem (e.g., Sahal-Bréchot 1974, 1977; House 1977).

Our treatment was based on the nonrelativistic quantum theory of line formation in a magnetized medium, put forward by Landi Degl'Innocenti (1983, 1984, 1985), which provides a very compact and powerful formalism (implementing the irreducible representation of spherical tensors) for the study of line-polarization problems, under the hypothesis of complete redistribution in frequency. Through this formalism, previous results on the linear polarization of coronal lines are easily rederived, whereas the new results on circular polarization presented in this paper are arrived at with relatively little effort.

The physical regimes of temperatures and magnetic intensities that are considered in this paper can be summarized by the following sequence of inequalities,

$$\omega_{\rm fs} \gg \Delta\omega_{\rm D} \gg \omega_{\rm L} \gg A_{\rm M1} \ , \tag{45}$$

where $\omega_{\rm fs}$ is the typical fine-structure separation in the ground term of the investigated ion, $\Delta\omega_{\rm D}$ is the typical Doppler width for the lines of interest [$\Delta\omega_{\rm D} \sim (v/c)\omega_{\rm fs}$, v being a typical thermal speed in the corona], $\omega_{\rm L}$ is the Larmor frequency for the magnetic intensities that are typical of the solar corona, and finally $A_{\rm M1}$ is the typical Einstein coefficient for spontaneous de-excitation for the lines of interest. Because $\omega_{\rm fs} \gg \omega_{\rm L} \gg A_{\rm M1}$, we were able to neglect quantum coherences in the ground term (higher terms are naturally populated and depopulated by isotropic collisional and radiative processes; see § 2.2). Because $\Delta\omega_{\rm D} \gg \omega_{\rm L}$, we were able to approximate the line-broadening profile through its first-order Taylor expansion in $\omega_{\rm L}$ (see § 2.3). Through this first-order approximation of the line profile, the magnetic-field strength is naturally introduced into the problem of coronal-line polarization, allowing for diagnosis of the magnetic-field intensities in the solar corona. In contrast, these magnetic, first-order effects were always neglected in previous work on the formation theory of coronal lines, so only the problem of the orientation of the magnetic field on the POS could be addressed.

We found that the consistent treatment of all four Stokes parameters in the investigation of the resonance scattering of the photospheric radiation, for the regimes of temperatures and magnetic intensities described by equation (45), leads to a generalization of the well-known "magnetograph formula," equation (40), relating the observed V profile to the frequency derivative of the intensity, I. The correction to the standard magnetograph formula is determined by the presence of atomic polarization—induced by the anisotropy of the incident radiation field and evaluated by the alignment factor of the excited level, $\sigma^2_0(\alpha_0 J)$—and is included in the magnetograph formula through an additional factor κ, ranging between 2/3 and 2 (for the two-level atom 1–0, in the absence of collisions) as a function of atomic alignment and magnetic-field geometry (see eq. [41], and discussion thereafter). Since atomic alignment can be large in the solar corona, depending on the height of the observed point over the limb and on the inclination of the magnetic field on the local vertical of the Sun at the observed point, we warn against a "blind" use of the standard magnetograph formula for the interpretation of the observed V signal as a direct diagnostic of the longitudinal magnetic field that simply ignores the possible deviations from the magnetograph regime of equation (40) determined by atomic polarization. The presence of isotropic collisions and cascade processes tends to reduce the alignment of the excited level, thus decreasing the relative importance of the correction to the magnetograph formula. While such depolarizing effects need to be considered individually for each line of interest and will be investigated in future papers of this series, the work of Judge (1998; specifically the lower panel of Fig. 1) can be used to indicate the likely magnitude of such effects. Certain lines (e.g., Fe XIII λ10747) have strong contributions to the intensity from radiative excitation for all heights in the corona and can potentially be expected to be strongly influenced by atomic alignment. Other lines (e.g., Si IX 3.934 μm) having large contributions from collisions low in the corona (below $h \sim 0.4\ R_\odot$) are expected to be less affected by atomic alignment, at least at low heights.

The authors wish to thank Egidio Landi Degl'Innocenti (Università di Firenze, Italy) for a careful reading of the manuscript and for helpful discussions. David Elmore (HAO) and Haosheng Lin (NSO) are gratefully acknowledged for providing relevant information on state-of-the-art polarization measurements in the solar corona. The anonymous referee is gratefully acknowledged for several comments that substantially improved the presentation of this work.

REFERENCES

Allen, C. W. 1973, Astrophysical Quantities (London: Athlone)
Arnaud, J. 1982, A&A, 112, 350
Arnaud, J., & Newkirk, G. N., Jr. 1987, A&A, 178, 263
Blum, K. 1981, Density Matrix Theory and Applications (New York: Plenum)
Brink, D. M., & Satchler, G. R. 1968, Angular Momentum (Oxford: Clarendon Press)
Charvin, P. 1965, Ann. Astrophys., 28, 877
Harvey, J. W. 1969, Ph.D. thesis, Univ. Colorado, Boulder
House, L. L. 1977, ApJ, 214, 632
Hyder, C. L. 1965, ApJ, 141, 1382
Judge, P. G. 1998, ApJ, 500, 1009
Kuhn, J. R. 1995, in IR Tools for Solar Astrophysics: What's Next?, ed. J. R. Kuhn & M. J. Penn (Singapore: World Scientific), 89
Lamb, F. K., & ter Haar, D. 1971, Phys. Rep., 2, 253
Landi Degl'Innocenti, E. 1982, Sol. Phys., 79, 291
Landi Degl'Innocenti, E. 1983, Sol. Phys., 85, 1 (LA83)
———. 1984, Solar Phys., 91, 1 (LA84)
———. 1985, Sol. Phys., 105, 1 (LA85)
Landi Degl'Innocenti, E., Bommier, V., & Sahal-Bréchot, S. 1991, A&A, 244, 391
Low, B. C., & Lou, Y. Q. 1990, ApJ, 352, 343
Parker, E. N. 1994, Spontaneous Current Sheets in Magnetic Fields with Application to Stellar X-Rays (Oxford: Oxford Univ. Press)
Perche, J. C. 1965, CR Acad. Sci. Paris, 260, 6036
———. 1965, CR Acad. Sci. Paris, 261, 5319
Querfeld, C. W., & Smartt, R. N. 1984, Sol. Phys., 91, 299
Sahal-Bréchot, S. 1974, A&A, 36, 355
———. 1977, ApJ, 213, 887
Van Ballegooijen, A. A. 1985, ApJ, 298, 421
Varshalovich, D. A., Moskalev, A. N., & Khersonskii, V. K. 1988, The Quantum Theory of Angular Momentum (Singapore: World Scientific)